

Cite this: *Chem. Sci.*, 2022, 13, 9366

All publication charges for this article have been paid for by the Royal Society of Chemistry

Mutual functionalization of dinitrogen and methane mediated by heteronuclear metal cluster anions CoTaC_2^-

Li-Hui Mou,^{†,ac} Yao Li,^{†,bc} Gong-Ping Wei,^{†,ac} Zi-Yu Li,^{*ac} Qing-Yu Liu,^{ac}
Hui Chen^{†,bc} and Sheng-Gui He^{†,ac}

The direct coupling of dinitrogen (N_2) and methane (CH_4) to construct the N–C bond is a fascinating but challenging approach for the energy-saving synthesis of N-containing organic compounds. Herein we identified a likely reaction pathway for N–C coupling from N_2 and CH_4 mediated by heteronuclear metal cluster anions CoTaC_2^- , which starts with the dissociative adsorption of N_2 on CoTaC_2^- to generate a $\text{Ta}^{\delta+}-\text{N}_t^{\delta-}$ (terminal-nitrogen) Lewis acid–base pair (LABP), followed by the further activation of CH_4 by $\text{CoTaC}_2\text{N}_2^-$ to construct the N–C bond. The $\text{N}\equiv\text{N}$ cleavage by CoTaC_2^- affording two N atoms with strong charge buffering ability plays a key part, which facilitates the $\text{H}_3\text{C}-\text{H}$ cleavage *via* the LABP mechanism and the N–C formation *via* a CH_3 migration mechanism. A novel N_t triggering strategy to couple N_2 and CH_4 molecules using metal clusters was accordingly proposed, which provides a new idea for the direct synthesis of N-containing compounds.

Received 29th April 2022

Accepted 13th July 2022

DOI: 10.1039/d2sc02416k

rsc.li/chemical-science

Introduction

The construction of N–C bonds directly from N_2 offers the potential to reduce the enormous fossil-fuel consumption for the current synthesis of N-containing organic compounds through NH_3 , which is mainly produced *via* the energy-intensive Haber–Bosch process ($\text{N}_2 + \text{H}_2 \rightarrow \text{NH}_3$).¹ Considerable research efforts have been devoted to this subject since the initial observation of N–C bond formation in the reaction of N_2 complexes with organic halides.² A long-sought goal for this chemistry has been the direct coupling of N_2 with abundant carbon-based molecules that are viable in industry. However, activation of these stable molecules remains a challenge, and only CO ,^{3–5} CO_2 ,^{6–8} and unsaturated hydrocarbons^{9,10} have been reported to form N–C bonds with N_2 induced by appropriate reactive species. CH_4 , the major component of widely available natural gas, is closely linked to industrial NH_3 synthesis in

which H_2 is produced through the energy-intensive CH_4 -reforming process. Therefore, the direct coupling of N_2 and CH_4 is of great importance for economic and environmental reasons. However, the appropriate species that can mediate the coupling of inert N_2 and CH_4 molecules to form an N–C bond has not been revealed.

Isolated gas-phase atomic clusters are important model systems for the precise design of desired active sites and the fundamental understanding of bond activation and formation processes.¹¹ The activation and individual functionalization of N_2 or CH_4 ,^{12–18} and the formation of N–C bonds^{19–25} are also extensively studied issues in the gas-phase field. Typical examples of N–C bond formation from N_2 or CH_4 in gas-phase studies can be classified as follows: (i) reactions of metal carbide clusters with N_2 ^{22–25} or metal nitride clusters with CH_4 ,^{26,27} and (ii) coupling reactions of CH_4 with NH_3 ^{28,29} or N_2 with CO_2 .⁶ In addition to reactions involving N_2 or CH_4 , the N–C bond formation was also observed in a few other reaction systems.^{30–32} Compared with these N–C formation processes, the direct coupling of N_2 and CH_4 is rather challenging and of particular interest.

Herein, we report the first example of N–C bond formation from the mutual functionalization of N_2 and CH_4 mediated by heteronuclear metal cluster anions CoTaC_2^- under thermal collision conditions. A terminal-nitrogen (N_t) triggering strategy for the coupling of N_2 and CH_4 was accordingly proposed (Scheme 1), which starts with the dissociative adsorption of N_2 on metal-based substrates to generate a $\text{M}^{\delta+}-\text{N}_t^{\delta-}$ Lewis acid–base pair (LABP), followed by the $\text{H}_3\text{C}-\text{H}$ cleavage of CH_4 *via* the LABP mechanism and the N–C formation *via* a CH_3 migration mechanism. Considering that

^aState Key Laboratory for Structural Chemistry of Unstable and Stable Species, Institute of Chemistry, Chinese Academy of Sciences, Beijing 100190, P. R. China. E-mail: shengguihe@iccas.ac.cn

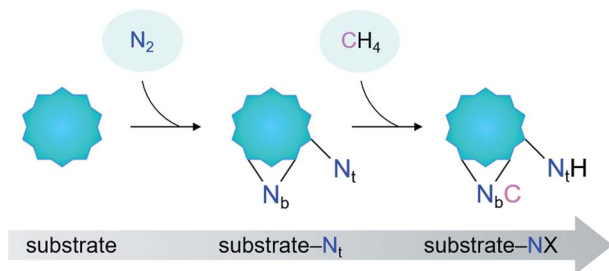
^bCAS Key Laboratory of Photochemistry, Institute of Chemistry, Chinese Academy of Sciences, Beijing 100190, P. R. China

^cBeijing National Laboratory for Molecular Sciences and CAS Research/Education Center of Excellence in Molecular Sciences, Beijing 100190, P. R. China

[†] Electronic supplementary information (ESI) available: Method details and additional experimental and theoretical results (spectra, data analysis, and calculated structures and reaction mechanisms). See <https://doi.org/10.1039/d2sc02416k>

^{*} Present address. University of Chinese Academy of Sciences, Beijing 100049, P. R. China.





Scheme 1 The proposed terminal-nitrogen (N_t) triggering strategy for the coupling of N_2 and CH_4 . The key to this strategy is the pre-dissociation of N_2 on an appropriate substrate to generate a N_t and a bridging-N (N_b).

the activation of CH_4 by some metal nitrides follows the LABP mechanism,^{26,27} we infer that the proposed strategy can be quite general, which is confirmed by the study on the $FeTaC_2^-/N_2/CH_4$ reaction system. The important roles of producing substrate- N_t complexes in the coupling of N_2 and CH_4 , as well as the strength of M- N_t bonds in the activity of the N_2 complexes were discussed.

Results

Cluster reactivity

The spectra in Fig. 1 have been obtained by using an online time-of-flight (TOF) mass spectrometer and show the results for

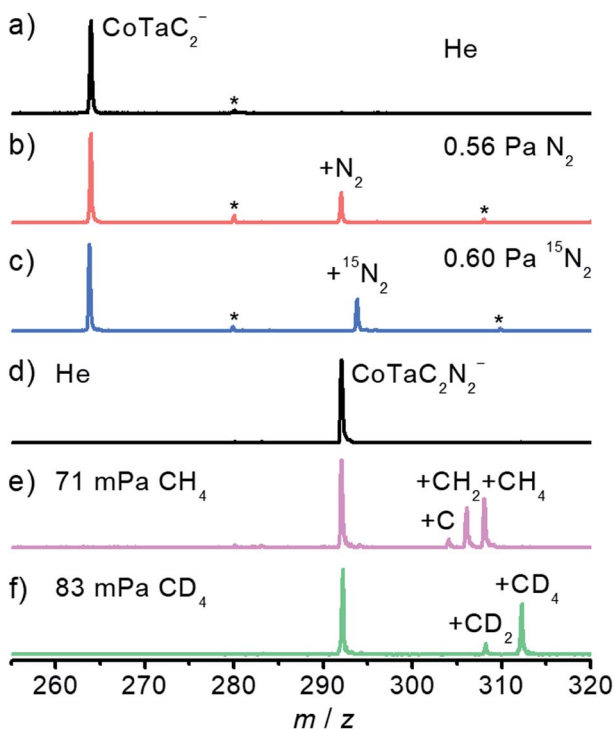


Fig. 1 Time-of-flight mass spectra of the reactions of $CoTaC_2^-$ with (a) He, (b) N_2 , and (c) $^{15}N_2$, and $CoTaC_2N_2^-$ with (d) He, (e) CH_4 , and (f) CD_4 . The reaction times are 4.8 ms for (b and c), 1.8 ms for (e), and 1.9 ms for (f). Peaks marked with asterisks are due to water impurities in the gas handling system.

the reactions of $CoTaC_2^-$ ($m/z = 264$) with N_2 and $CoTaC_2N_2^-$ ($m/z = 292$) with CH_4 . Reference spectra with inert He as the reactant gas were also recorded (Fig. 1a and d). The $CoTaC_2^-$ ions were generated by laser ablation of a mixed Co-Ta disk target (molar ratio Co/Ta = 2 : 1) in the presence of 0.05% CD_4 diluted with He carrier gas, and then mass-selected and thermalized to room temperature to react with N_2 in a linear ion trap (LIT) reactor. As shown in Fig. 1b, on pulsing 0.56 Pa N_2 into the LIT reactor, a strong product peak assigned as $CoTaC_2N_2^-$ appeared, suggesting the following reaction channel:



The isotopic labeling experiment using $^{15}N_2$ as the reactant gas (Fig. 1c) confirmed the above reaction channel. We should mention in passing that, a very tiny metal atom ejection channel (less than 1%) producing $TaC_2N_2^-$ was also observed (Fig. S1a-c†). Based on a least-squares fitting procedure (Fig. S2a†), the rate constant $k_1(CoTaC_2^-/N_2)$ of the pseudo first-order reaction between $CoTaC_2^-$ and N_2 was estimated to be $(8.0 \pm 1.6) \times 10^{-13} \text{ cm}^3 \text{ molecule}^{-1} \text{ s}^{-1}$, corresponding to a reaction efficiency ($\Phi = k_1/k_c$) of about 0.1% relative to the theoretical collision rate (k_c).³³

To study the reaction of the N_2 association product $CoTaC_2N_2^-$ with CH_4 , a newly-developed double ion trap apparatus (Scheme S1 in the ESI†) was used to first generate the $CoTaC_2N_2^-$ from the reaction of $CoTaC_2^-$ with N_2 in the first LIT reactor and then mass select $CoTaC_2N_2^-$ to interact with CH_4 in the second LIT reactor. Upon the interaction of $CoTaC_2N_2^-$ with CH_4 (Fig. 1e), three product peaks assigned as $CoTaC_2N_2CH_4^-$ ($m/z = 308$), $CoTaC_2N_2CH_2^-$ ($m/z = 306$), and $CoTaC_2N_2C^-$ ($m/z = 304$) were observed, suggesting the following reaction channels:



The rate constant $k_1(CoTaC_2N_2^-/CH_4)$ for the reaction of $CoTaC_2N_2^-$ with CH_4 was estimated to be $(1.4 \pm 0.3) \times 10^{-11} \text{ cm}^3 \text{ molecule}^{-1} \text{ s}^{-1}$, corresponding to a Φ of about 1.4%. Noticeably, the reaction channel of ejecting two D_2 molecules was negligible when using isotope-labeled CD_4 in place of CH_4 (Fig. 1f). The branching ratio of reaction channel (2) to reaction channel (3) changed to 80 : 20 in the CD_4 experiment, and the intermolecular kinetic isotopic effect (KIE) calculated using $k_1(CoTaC_2N_2^-/CH_4)/k_1(CoTaC_2N_2^-/CD_4)$ was estimated to be 1.3 (Fig. S2b and c†). The loss of H_2 (D_2) in the reaction of $CoTaC_2N_2^-$ with CH_4 (CD_4) suggests that activation of C-H bonds must have occurred. To determine the mechanisms of $CoTaC_2^- + N_2$ and $CoTaC_2N_2^- + CH_4$ reactions, structural characterization of the reactant cluster ions should be performed.



Structural characterization

Photoelectron imaging spectroscopy (PEIS)³⁴ combined with quantum chemistry calculations was employed to characterize the structures of CoTaC_2^- and $\text{CoTaC}_2\text{N}_2^-$. The structures were optimized at the density functional theory (DFT) level,³⁵ and their relative energies were then refined by high-level RCCSD(T) (partially spin-adapted open-shell coupled cluster method with single, double, and perturbative triple excitations) and DMRG-SC-NEVPT2 (density matrix renormalization group strongly-contract n -electron valence perturbation theory) methods.^{36,37}

The experimental spectrum of CoTaC_2^- recorded with 670 nm photons at 10 K reveals a sharp peak centered at 1.63 eV, followed by three discernible peaks with electron binding energies of 1.70, 1.73, and 1.76 eV (Fig. 2a, top). The calculated lowest-lying isomer ($^2\text{IS1}$) of CoTaC_2^- features a Co-Ta double bond with a Wiberg bond index (WBI) of 2.04 and a C_2 ligand. The presence of two d-d bonding orbitals between Co and Ta atoms provides further evidence for the Co-Ta double bond (Fig. S12†). The Franck-Condon (FC)-simulated spectrum of the $^2\text{A} \rightarrow ^3\text{A}$ vibrational transition for $^2\text{IS1}$ can reasonably reproduce the experimental spectrum from 1.70 to 1.76 eV (Fig. 2a, middle),³⁸ and the calculated adiabatic electron detachment energy (ADE) of $^2\text{IS1}$ is close to the experimental value (1.83 eV

vs. 1.70 eV), suggesting that $^2\text{IS1}$ is the most probable species of CoTaC_2^- generated in the experiment. The first spectral peak centered at 1.63 eV might come from the minor population of the isomer $^4\text{IS2}$ with a relative energy of 0.59 eV higher than $^2\text{IS1}$, considering that its calculated ADE (1.59 eV) and simulated profile of the $^4\text{A} \rightarrow ^3\text{A}$ transition match well with the first spectral peak (Fig. 2a, bottom). A more detailed discussion of the structural assignment of CoTaC_2^- is provided in the ESI (Fig. S3†).

Reaction mechanism for the $\text{CoTaC}_2^-/\text{N}_2$ couple

The reaction pathway of CoTaC_2^- ($^2\text{IS1}$) with N_2 calculated at the RCCSD(T) level is shown in Fig. 2b. The N_2 molecule first approaches the Ta atom through a side-on (η^2) mode to form the encounter complex $^2\text{I1}$ (−0.47 eV). Further binding of N_2 to Co is impeded by a high energy barrier with the doublet spin state ($^2\text{TS1}/0.10$ eV); however, this process can be accomplished through transiting to the quartet spin state ($^4\text{TS1}/-0.13$ eV) and then a more stable intermediate $^2\text{I2}$ (−0.84 eV) with a side-on-end-on ($\eta^2:\eta^1$) bounded N_2 unit is formed. By surmounting $^2\text{TS2}$, N_2 is coordinated to the Co-Ta center in a distorted- $\eta^2:\eta^1$ mode ($^2\text{I3}/-0.64$ eV) with an N-N bond length of 135 pm. The N-N bond is disrupted entirely after overcoming a slight energy barrier of 0.11 eV ($^2\text{TS3}/-0.53$ eV), yielding one terminal-N (N_t) and one bridging-N (N_b) in $^2\text{I4}$ (−1.39 eV). The subsequent N- $\text{C}_{\text{cluster}}$ coupling would encounter a highly positive energy barrier ($^2\text{TS17}/0.10$ eV, Fig. S4†) that has little chance of being surmounted under thermal collision conditions, and thus the $^2\text{I4}$ would be stabilized as the adsorption product $\text{CoTaC}_2\text{N}_2^-$ through collisions with bath gas He. Note that the very minor reaction channel of generating TaC_2N_2^- in the reactivity experiment might come from the reaction of the high-lying isomer $^4\text{IS2}$ with N_2 , in which two steps of N- $\text{C}_{\text{cluster}}$ coupling take place before ejecting a neutral Co atom (Fig. S5†).

The PEIS characterization of $\text{CoTaC}_2\text{N}_2^-$ at different reaction temperatures and photon energies supported the assignment of $^2\text{I4}$ as the adsorption product and also proved the reliability of our RCCSD(T) calculations. As shown in Fig. 2c, only one spectral peak (B) was observed in the experimental spectrum recorded with 410 nm photons at 250 K (note that the residual water in the room-temperature ion trap will deplete the CoTaC_2^- signal under the condition of a long trapping time of 80 ms, so the room-temperature reaction was not performed in the PEIS experiment); however, two spectral peaks (A and B) could be observed when the reaction temperature decreased to 200 K and 170 K. This implies that an additional intermediate was stabilized as the adsorption product $\text{CoTaC}_2\text{N}_2^-$ at lower temperatures and accounted for the appearance of peak A. Considering that the process of $^2\text{I1} \rightarrow ^4\text{TS1} \rightarrow ^2\text{I2}$ with the highest energy barrier and a spin crossing³⁹ is the rate-limiting step (Fig. 2b), $^2\text{I1}$ is the most probable species that could be stabilized at lower temperatures. When the temperature is decreased to a certain value, all of the I1 might be stabilized and cannot transform into I4 . However, this situation is not the focus of this work because we aim to study the reactions of $\text{CoTaC}_2^-/\text{N}_2$ and $\text{CoTaC}_2\text{N}_2^-/\text{CH}_4$ couples at room temperature.

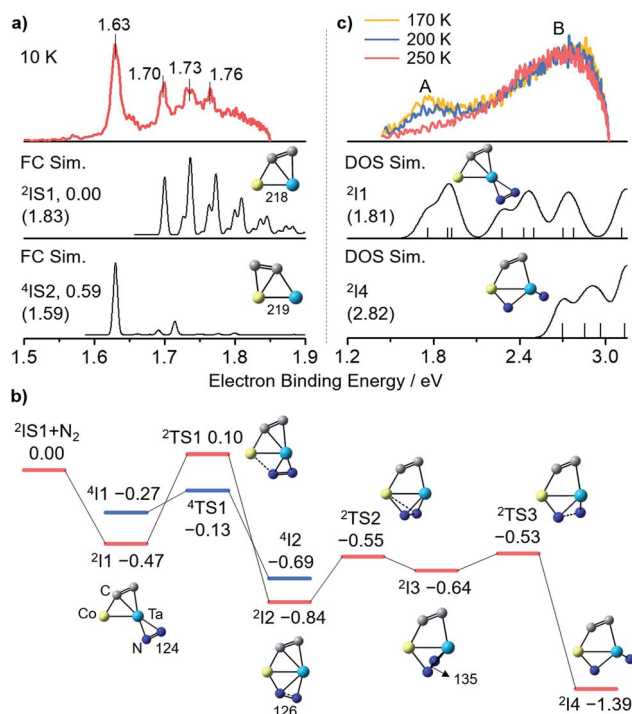


Fig. 2 (a) Experimental and Franck-Condon (FC)-simulated photoelectron spectra of CoTaC_2^- . (b) RCCSD(T)-calculated potential energy profile for the reaction of CoTaC_2^- ($^2\text{IS1}$) with N_2 . (c) Experimental and density of states (DOS)-simulated photoelectron spectra of $\text{CoTaC}_2\text{N}_2^-$. The 670 nm (1.85 eV) and 410 nm (3.02 eV) photons were used for CoTaC_2^- and $\text{CoTaC}_2\text{N}_2^-$, respectively. The relative energies, ADEs and VDEs (in brackets) are given in eV. The bond lengths are in pm. The superscripts indicate spin multiplicities. The simulated spectra of $^2\text{IS1}$, $^2\text{I1}$, $^2\text{I4}$ and $^4\text{IS2}$ are red shifted by 0.13, 0.05, 0.12 eV and blue shifted by 0.04 eV, respectively.



The simulated spectra of $\text{CoTaC}_2\text{N}_2^-$ isomers based on density of states (DOS) simulations⁴⁰ confirmed the contribution of $^2\text{I1}$ to peak A and indicated that peak B in the 250 K spectrum was contributed by $^2\text{I4}$ (Fig. 2c). Moreover, the employment of 365 nm photons for the PEIS characterization of $\text{CoTaC}_2\text{N}_2^-$ provides further evidence for the agreement of the DOS-simulated spectrum of $^2\text{I4}$ with the experimental one (Fig. S6b and d†). Other $\text{CoTaC}_2\text{N}_2^-$ isomers with the N–N or N–C bonds should be excluded due to their mismatched VDE values and spectral patterns with the experimental spectrum (Fig. S6e–k†) and their theoretically predicted inertness toward CH_4 (Fig. S7†). Therefore, a N_t -containing complex was successfully prepared through the dissociative adsorption of N_2 on CoTaC_2^- at room temperature.

Reaction mechanism for the $\text{CoTaC}_2\text{N}_2^-/\text{CH}_4$ couple

As shown in Fig. 3, the $\text{CoTaC}_2\text{N}_2^-$ ($^2\text{I4}$) interacts with CH_4 by first anchoring it on the Ta atom to form $^2\text{I5}$ with a binding energy of 0.44 eV. The first $\text{H}_3\text{C}-\text{H}$ bond cleavage preferably proceeds *via* the cooperative mechanism of a LABP composed of Ta (natural charge: 1.31e) and N_t (natural charge: -0.79e) atoms, generating a N_t-H bond and a Ta– CH_3 moiety in $^2\text{I6}$ (-2.52 eV). After that, the CH_3 group tends to migrate from Ta to N_b to liberate the Ta site ($^2\text{I6} \rightarrow ^2\text{TS5} \rightarrow ^2\text{I7}$). On the basis of Rice–Ramsperger–Kassel–Marcus (RRKM) theory,⁴¹ the conversion rate of $^2\text{I6} \rightarrow ^2\text{TS5}$ is estimated to be $6.9 \times 10^4 \text{ s}^{-1}$, which is

one order of magnitude smaller than the collision rate ($6.7 \times 10^5 \text{ s}^{-1}$) that a cluster experiences with the bath gas He in the LIT reactor. This suggests that only a small part of $^2\text{I6}$ could overcome $^2\text{TS5}$ to form $^2\text{I7}$, while most of the $^2\text{I6}$ would be stabilized as the adsorption product $\text{CoTaC}_2\text{N}_2\text{CH}_4^-$ through collisions with bath gas. If the barrier height of $^2\text{TS5}$ is decreased by 0.1 eV, which could be the uncertainty of RCCSD(T) calculations,⁴² the rate of $^2\text{I6} \rightarrow ^2\text{TS5}$ is increased to $3.3 \times 10^5 \text{ s}^{-1}$, which is of the same order of magnitude as the collision rate and can lead to the stabilization of about half of the $^2\text{I6}$ (P1) as $\text{CoTaC}_2\text{N}_2\text{CH}_4^-$. This agrees well with the ratio of $\text{CoTaC}_2\text{N}_2\text{CH}_4^-$ to $\text{CoTaC}_2\text{N}_2\text{CH}_2\text{O}^-$ (49 : 51) in the reactivity experiment (Fig. 1).

After the formation of $^2\text{I7}$, the reaction proceeds with a H atom of the CH_3 group transferred to the Ta atom to form $^2\text{I8}$. The resultant CH_2 unit then forms a chemical bond with the Co atom, enabling the consecutive activation of the remaining two C–H bonds *via* the transfer of H atoms to Co ($^2\text{I9} \rightarrow ^2\text{I10} \rightarrow ^2\text{I11}$). Along with two steps of structural rearrangements ($^2\text{I11} \rightarrow ^2\text{I12} \rightarrow ^2\text{I13}$), two H atoms on Co make a H_2 unit to generate the lowest-lying isomer ($^2\text{IS3}$) of $\text{CoTaC}_2\text{N}_2\text{CH}_2^-$ concomitant with loss of H_2 . The RRKM-theory calculated rates of traversing $^2\text{TS6}-^2\text{TS11}$ and H_2 desorption from $^2\text{I13}$ are at least two orders of magnitude larger than the collision rate (ESI Table 3†), indicating the impossible stabilization of intermediates $^2\text{I7}-^2\text{I13}$ and the facile formation of $^2\text{IS3}$. The generation of P2

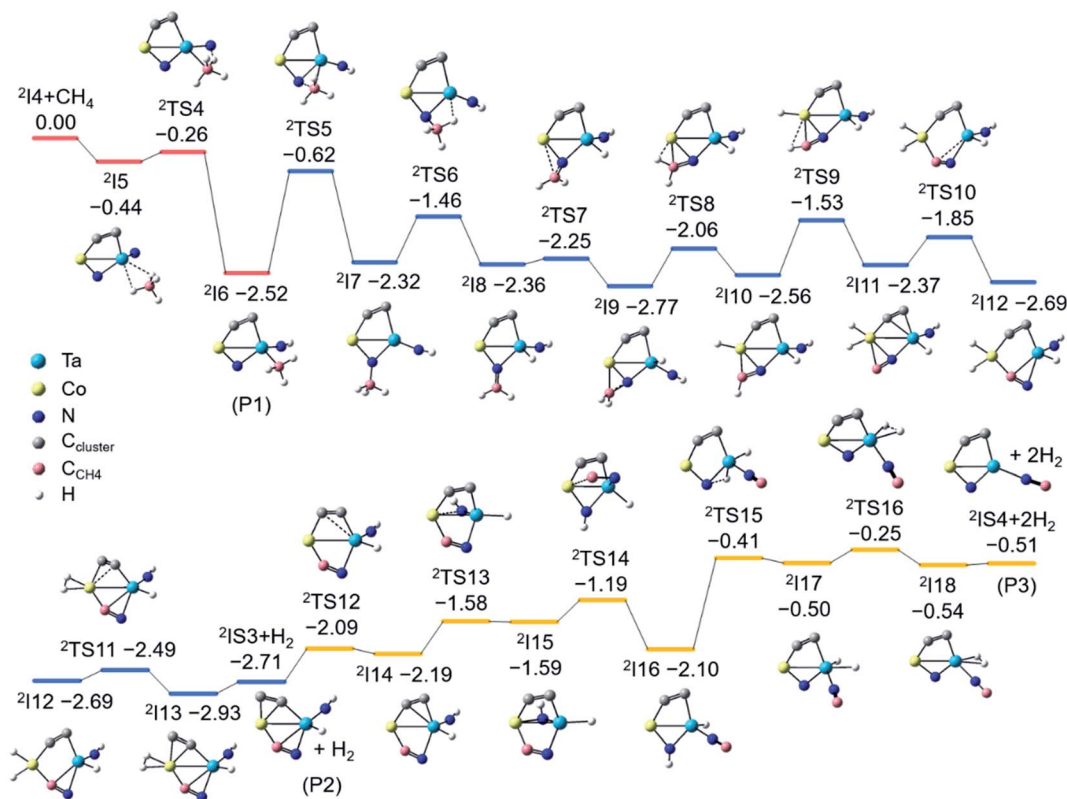


Fig. 3 Potential energy profile for the reaction of $\text{CoTaC}_2\text{N}_2^-$ ($^2\text{I4}$) with CH_4 . The structures are optimized at the DFT level. The zero-point vibration corrected energies in eV relative to the separated reactants are calculated at the RCCSD(T) level. The C atoms from CoTaC_2^- and CH_4 are shown in different colours.



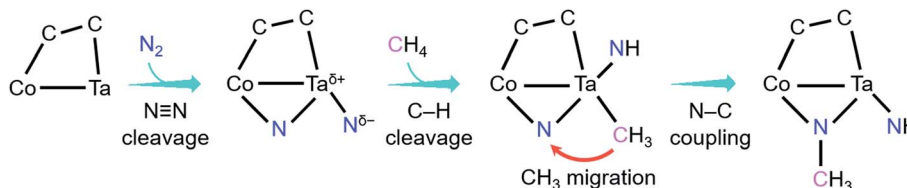


Fig. 4 Key events and mechanisms for the coupling reaction of N_2 with CH_4 mediated by $CoTaC_2^-$ cluster anions.

($^2IS3 + H_2$) is highly exothermic (-2.71 eV), so 2IS3 has enough internal energy to undergo further transformation to evaporate the second H_2 molecule and yield the lowest-lying isomer (2IS4) of $CoTaC_2N_2C^-$ (Fig. S8†). The most favorable pathway to generate P3 ($^2IS4 + H_2$) from 2IS3 involves a Co–NH bond-forming process ($^2I14 \rightarrow ^2I15$) and a Co–CN bond-breaking process ($^2I15 \rightarrow ^2I16$), followed by the transfer of a H atom from N to Ta to generate 2I17 , from which a H_2 molecule can be evaporated. The above high-level RCCSD(T) calculations indicate that the N– C_{CH_4} bond is formed in the dehydrogenation product $CoTaC_2N_2CH_{2,0}^-$. Note that it is very difficult to perform the PEIS characterization of $CoTaC_2N_2CH_{4,2,0}^-$ with the current apparatus due to the very weak signals of these species and the mass overlap with other species such as $CoTaC_4H_2O^-$ and $CoTaC_2ON_2^-$ (Fig. S9†). Quantum chemistry calculations confirmed that the formation of the N– C_{CH_4} bond is necessary for the experimentally observed reactions and the migration of the CH_3 group from Ta to N_b is the most favorable pathway.

Discussion

As shown in Fig. 4, the coupling reaction of N_2 with CH_4 mediated by $CoTaC_2^-$ starts with cleavage of the $N\equiv N$ bond by $CoTaC_2^-$ to generate $CoTaC_2N_2^-$ with a $Ta^{\delta+}-Nb^{\delta-}$ LBP, followed by further activation of CH_4 by $CoTaC_2N_2^-$, in which the first C–H bond is cleaved *via* a $Ta^{\delta+}-Nb^{\delta-}$ LBP mechanism and the N–C coupling is subsequently achieved *via* a CH_3 migration mechanism. The order of activation of the two molecules is crucial to this coupling reaction, as reflected by the low reactivity of $CoTaC_2^-$ toward CH_4 to produce $CoTaC_3H_2^-$ (Fig. S1d and e,† $k_1 = 1.2 \times 10^{-14}$ cm^3 molecule $^{-1}$ s $^{-1}$) and the theoretically predicted impossibility of functionalizing N_2 by $CoTaC_3H_2^-$ (Fig. S10c†). Comparative studies on $CoTaC_2^-/CH_4$ and $CoTaC_2N_2^-/CH_4$ reaction couples indicate that the approach of CH_4 to $CoTaC_2N_2^-$ is overall barrierless, while the approach of CH_4 to $CoTaC_2^-$ encounters a positive energy barrier of 0.05 eV (Fig. S10a†). Moreover, cleavage of the H_3C-H bond by $CoTaC_2^-$ follows the oxidative addition mechanism, which is kinetically less favorable than the LBP mechanism in the $CoTaC_2N_2^-/CH_4$ couple (Fig. S10b†). Therefore, the design of first activating N_2 not only constructs a $Ta^{\delta+}-Nb^{\delta-}$ LBP to facilitate the initial activation of CH_4 , but also generates a sufficiently reactive N_b atom that can accept the migrating CH_3 group to form the N–C bond.

Natural charge analysis of the $CoTaC_2N_2^-/CH_4$ reaction system reveals that the two N atoms in $CoTaC_2N_2^-$ exhibit

strong charge buffering ability throughout the activation of CH_4 : they store a large number of negative charges ($\Delta Q = -0.47e$) during the processes of H_3C-H cleavage (N_t-H formation) and N_b-C formation, while releasing all of the stored negative charges ($\Delta Q = 0.52e$) during the activation of the remaining three C–H bonds (Fig. S11†). Such charge buffering behavior largely reduces the kinetic barriers of rate-limiting steps and thus drives the N–C bond formation. Noticeably, the N–C bond formation from N_2 outlined here differs fundamentally from that in previous gas-phase studies. Generally, the carbon ligands in transition metal carbide clusters, such as $FeTaC_2^-$, $FeV_2C_2^-$, $V_3C_4^-$, and $Ta_2C_4^-$, were employed to construct N– $C_{cluster}$ bonds after the $N\equiv N$ bond was completely cleaved by the metal center.^{22–25} This study provides a likely pathway for N–C bond formation from the product of N_2 cleavage through migrating a CH_4 -derived CH_3 group to a N_2 -derived N atom, which opens a new window for the reactions of N_2 -derived metal nitrides.

Finally, we infer that N_2 -derived metal nitrides with a $M-N_t$ LBP might be promising species for further activation of CH_4 . As expected, the previously reported $FeTaC_2N_2^-$ with a similar $Ta^{\delta+}-Nb^{\delta-}$ LBP (natural charge: $1.33e/-0.89e$) is demonstrated to react with CH_4 to produce $FeTaC_2N_2CH_4^-$ and $FeTaC_2N_2CH_2^-$ (ratio = 70 : 30) by using a newly-designed ship-lock-type reactor (Fig. S13†).⁴³ More interestingly, the reaction rate of the $FeTaC_2N_2^-/CH_4$ couple ($k_1 = 2.8 \times 10^{-15}$ cm^3 molecule $^{-1}$ s $^{-1}$) is about four orders of magnitude smaller than that of $CoTaC_2N_2^-/CH_4$ couple, indicating a large difference in the initial activation of CH_4 by the $Ta^{\delta+}-Nb^{\delta-}$ LBP. A key difference between the two systems is that the degree of N_2 reduction by $CoTaC_2^-$ is properly reduced compared to $FeTaC_2^-$, as reflected by fewer negative charges on N atoms and smaller electron occupancy on N_{2p} orbitals in $CoTaC_2N_2^-$ than those in $FeTaC_2N_2^-$ (Fig. S14†). This leads to a slightly weaker $Ta-N_t$ bond in $CoTaC_2N_2^-$ (WBI: 2.4) than that in $FeTaC_2N_2^-$ (WBI: 2.6), which has more possibility to buffer the charge variation during the initial H_3C-H cleavage process. This agrees with the fact that it is difficult for N_2 -derived nitrides with strong M–N bonds to activate other molecules. Further research on the optimal design of highly reactive $M^{\delta+}-N_t^{\delta-}$ LBP during the activation of N_2 to trigger efficient N–C coupling in the further activation of CH_4 is in progress.

Conclusions

A possible N–C bond formation from the mutual functionalization of N_2 and CH_4 mediated by heteronuclear metal cluster



anions CoTaC_2^- was studied by using mass spectrometry, photoelectron spectroscopy and a modelled reaction pathway. As verified by employing mass spectrometry, photoelectron imaging spectroscopy, and quantum chemistry calculations, the coupling reaction of N_2 with CH_4 starts with the dissociative adsorption of N_2 on CoTaC_2^- to generate a $\text{Ta}^{\delta+}-\text{N}_t^{\delta-}$ Lewis acid–base pair, which then triggers the $\text{H}_3\text{C}-\text{H}$ cleavage (N_t-H formation) and $\text{N}-\text{C}_{\text{CH}_4}$ formation in the reaction of $\text{CoTaC}_2\text{N}_2^-$ with CH_4 . Cleaving the $\text{N}\equiv\text{N}$ bond to generate two N atoms with large charge buffer capacity underlies the ability of CoTaC_2^- to mediate the coupling of N_2 and CH_4 . Based on this finding, a universal N_t triggering strategy was proposed to couple inert N_2 and CH_4 molecules, which may inspire the rational design of catalysts to produce N-containing organic compounds.

Author contributions

L.-H. M. and S.-G. H. conceived the ideas. L.-H. M. carried out the experiments and calculations and wrote the original manuscript. Y. L. and H. C. assisted with high-level quantum calculations. G. P. W. and Q.-Y. L. assisted with the experiments. S.-G. H., Z.-Y. L. and H. C. supervised the results and commented on the manuscript.

Conflicts of interest

There are no conflicts to declare.

Acknowledgements

This work was supported by the National Natural Science Foundation of China (Grants 21833011, 22173111 and 92161205), the Youth Innovation Promotion Association CAS (No. 2020034), and the K. C. Wong Education Foundation.

References

- 1 S. Kim, F. Loose and P. J. Chirik, *Chem. Rev.*, 2020, **120**, 5637–5681.
- 2 J. Chatt, A. A. Diamantis, G. A. Heath, N. E. Hooper and G. J. Leigh, *J. Chem. Soc., Dalton Trans.*, 1977, 7, 688–697.
- 3 D. J. Knobloch, E. Lobkovsky and P. J. Chirik, *Nat. Chem.*, 2010, **2**, 30–35.
- 4 S. P. Semproni and P. J. Chirik, *J. Am. Chem. Soc.*, 2013, **135**, 11373–11383.
- 5 Z. J. Lv, Z. Huang, W. X. Zhang and Z. Xi, *J. Am. Chem. Soc.*, 2019, **141**, 8773–8777.
- 6 M. Wang, L.-Y. Chu, Z.-Y. Li, A. M. Messinis, Y.-Q. Ding, L. Hu and J.-B. Ma, *J. Phys. Chem. Lett.*, 2021, **12**, 3490–3496.
- 7 Y. Nakanishi, Y. Ishida and H. Kawaguchi, *Angew. Chem., Int. Ed.*, 2017, **56**, 9193–9197.
- 8 D. J. Knobloch, H. E. Toomey and P. J. Chirik, *J. Am. Chem. Soc.*, 2008, **130**, 4248–4249.
- 9 S. F. McWilliams, D. L. J. Broere, C. J. V. Halliday, S. M. Bhutto, B. Q. Mercado and P. L. Holland, *Nature*, 2020, **584**, 221–226.
- 10 L. Morello, J. B. Love, B. O. Patrick and M. D. Fryzuk, *J. Am. Chem. Soc.*, 2004, **126**, 9480–9481.
- 11 S. M. Lang and T. M. Bernhardt, *Phys. Chem. Chem. Phys.*, 2012, **14**, 9255–9269.
- 12 L.-H. Mou, G.-D. Jiang, Z.-Y. Li and S.-G. He, *Chin. J. Chem. Phys.*, 2020, **33**, 507–520.
- 13 Y.-X. Zhao, Z.-Y. Li, Y. Yang and S.-G. He, *Acc. Chem. Res.*, 2018, **51**, 2603–2610.
- 14 H. Schwarz, S. Shaik and J. Li, *J. Am. Chem. Soc.*, 2017, **139**, 17201–17212.
- 15 D. V. Fries, M. P. Klein, A. Steiner, M. H. Prosenec and G. Niedner-Schatteburg, *Phys. Chem. Chem. Phys.*, 2021, **23**, 11345–11354.
- 16 F. Mafune, Y. Tawarayama and S. Kudoh, *J. Phys. Chem. A*, 2016, **120**, 4089–4095.
- 17 G. Liu, I. R. Ariyaratna, S. M. Ciborowski, Z. Zhu, E. Miliordos and K. H. Bowen, *J. Am. Chem. Soc.*, 2020, **142**, 21556–21561.
- 18 N. Levin, J. Lengyel, J. F. Eckhard, M. Tschurl and U. Heiz, *J. Am. Chem. Soc.*, 2020, **142**, 5862–5869.
- 19 R. Kretschmer, M. Schlangen and H. Schwarz, *Understanding Organometallic Reaction Mechanisms and Catalysis*, ed. V. P. Ananikov, Wiley-VCH, Weinheim, 2014, pp. 1–16.
- 20 S. Zhou, J. Li, M. Schlangen and H. Schwarz, *Acc. Chem. Res.*, 2016, **49**, 494–502.
- 21 R. Kretschmer, M. Schlangen, M. Kaupp and H. Schwarz, *Organometallics*, 2012, **31**, 3816–3824.
- 22 L.-H. Mou, Y. Li, Z.-Y. Li, Q.-Y. Liu, H. Chen and S.-G. He, *J. Am. Chem. Soc.*, 2021, **143**, 19224–19231.
- 23 L.-H. Mou, Y. Li, Z.-Y. Li, Q.-Y. Liu, H. Chen and S.-G. He, *J. Phys. Chem. Lett.*, 2020, **11**, 9990–9994.
- 24 Z.-Y. Li, Y. Li, L.-H. Mou, J.-J. Chen, Q.-Y. Liu, S.-G. He and H. Chen, *J. Am. Chem. Soc.*, 2020, **142**, 10747–10754.
- 25 Z.-Y. Li, L.-H. Mou, G.-P. Wei, Y. Ren, M.-Q. Zhang, Q.-Y. Liu and S.-G. He, *Inorg. Chem.*, 2019, **58**, 4701–4705.
- 26 S. Zhou, J. Li, M. Schlangen and H. Schwarz, *Angew. Chem., Int. Ed.*, 2016, **55**, 14863–14866.
- 27 S. Zhou, J. Li, M. Schlangen and H. Schwarz, *Angew. Chem., Int. Ed.*, 2016, **55**, 11678–11681.
- 28 K. Koszinowski, D. Schroder and H. Schwarz, *J. Am. Chem. Soc.*, 2003, **125**, 3676–3677.
- 29 M. Diefenbach, M. Brönstrup, M. Aschi, D. Schröder and H. Schwarz, *J. Am. Chem. Soc.*, 1999, **121**, 10614–10625.
- 30 R. Kretschmer, M. Schlangen and H. Schwarz, *Angew. Chem., Int. Ed.*, 2011, **50**, 5387–5391.
- 31 R. Kretschmer, M. Schlangen and H. Schwarz, *Angew. Chem., Int. Ed.*, 2012, **51**, 3483–3488.
- 32 M. Schlangen, J. Neugebauer, M. Reiher, D. Schröder, J. P. López, M. Haryono, F. W. Heinemann, A. Grohmann and H. Schwarz, *J. Am. Chem. Soc.*, 2008, **130**, 4285–4294.
- 33 G. Gioumousis and D. P. Stevenson, *J. Chem. Phys.*, 1958, **29**, 294–299.
- 34 Q.-Y. Liu, L. Hu, Z.-Y. Li, C.-G. Ning, J.-B. Ma, H. Chen and S.-G. He, *J. Chem. Phys.*, 2015, **142**, 164301.
- 35 J. Kohanoff and N. I. Gidopoulos, *Handbook of Molecular Physics and Quantum Chemistry*, ed. S. Wilson, John Wiley & Sons, Ltd, Chichester, 2003, pp. 532–568.



- 36 J. D. Watts, J. Gauss and R. J. Bartlett, *J. Chem. Phys.*, 1993, **98**, 8718–8733.
- 37 S. Guo, M. A. Waston, W. F. Hu, Q. M. Sun and G. K. L. Chan, *J. Chem. Theory Comput.*, 2016, **12**, 1583–1591.
- 38 V. Mozhayskiy and A. I. Krylov, *ezSpectrum v3.0*, see <https://iopshell.usc.edu/downloads>.
- 39 D. Schroder, S. Shaik and H. Schwarz, *Acc. Chem. Res.*, 2000, **33**, 139–145.
- 40 D. J. Tozer and N. C. Handy, *J. Chem. Phys.*, 1998, **109**, 10180–10189.
- 41 J. I. Steinfeld, J. S. Francisco and W. L. Hase, *Chemical Kinetics and Dynamics*. Prentice-Hall, Upper Saddle River, NJ, 1999, pp. 231–313.
- 42 W. Jiang, N. J. DeYonker and A. K. Wilson, *J. Chem. Theory Comput.*, 2012, **8**, 460–468.
- 43 G.-P. Wei, Q.-Y. Liu, Y. Ren and S.-G. He, *Rev. Sci. Instrum.*, 2021, **92**, 104104.

